Generalized Fulde-Ferrell-Larkin-Ovchinnikov state in heavy-fermion and intermediate-valence systems

M. Tachiki, S. Takahashi, Philipp Gegenwart, M. Weiden, M. Lang, C. Geibel, F. Steglich, R. Modler, C. Paulsen, Y. Ōnuki

Angaben zur Veröffentlichung / Publication details:

Tachiki, M., S. Takahashi, Philipp Gegenwart, M. Weiden, M. Lang, C. Geibel, F. Steglich, R. Modler, C. Paulsen, and Y. Ōnuki. 1997. "Generalized Fulde-Ferrell-Larkin-Ovchinnikov state in heavy-fermion and intermediate-valence systems." *Zeitschrift für Physik B Condensed Matter* 100 (3): 369–80. https://doi.org/10.1007/s002570050135.

Generalized Fulde-Ferrell-Larkin-Ovchinnikov state in heavy-fermion and intermediate-valence systems

M. Tachiki[1], S. Takahashi[1], P. Gegenwart[2], M. Weiden[2], M. Lang[2], C. Geibel[2], F. Steglich[2], R. Modler[2,3], C. Paulsen[4], Y. Ōnuki[5]

[1] Institute for Materials Research, Tohoku University, 2-1-1 Katahira, Aoba-ku, Sendai 980, Japan
(Fax: +81-22 215 2006, Tel. +81-22-215-2005)
[2] Institut für Festkörperphysik, Technische Hochschule Darmstadt, Hochschulstrasse 8, D-64289 Darmstadt, Germany
(Fax: +49-6151-16 48 83, Tel.: +49-6151-16 21 84)
[3] Forschungszentrum Karlsruhe GmbH, INFP, D-76021 Karlsruhe, Germany
[4] CRTBT, CNRS, 38042 Grenoble Cedex 9, France
[5] Department of Physics, Osaka University, Toyonaka, Osaka 560, Japan

Abstract. Anomalous properties of the magnetization, the crystal dilatation, and other physical quantities observed in the mixed state of compounds such as UPd_2Al_3 and $CeRu_2$ suggest the occurrence of a new state near H_{c2}. In such compounds with large spin susceptibility and high H_{c2}, a new inhomogeneous superconducting state is theoretically predicted to occur in high magnetic fields. In this inhomogeneous state which is shown to be a generalized Fulde-Ferrell-Larkin-Ovchinnikov state, the order parameter is spatially modulated, and planar nodes of the order parameter are periodically aligned perpendicular to the vortices. Various theoretical predictions are compared with experimental results on UPd_2Al_3 and $CeRu_2$ related to this new superconducting high-field state.

1. Introduction

Modler et al. [1] have reported some time ago anomalies in the sample length within the superconducting state of the Heavy-Fermion superconductor UPd_2Al_3 pointing to a first-order phase transition at 10 kOe $< H < H_{c2}$ and $T < 0.8T_c$. Gloos et al. [2] subsequently discussed these anomalies in view of a first-order phase transition from the mixed state to an inhomogeneous superconducting state as theoretically proposed by Fulde and Ferrell [3] and, independently, Larkin and Ovchinnikov [4].

Figure 1 shows a most recent experiment on the isothermal magnetization $M(H)$ at $T = 150$ mK of the same UPd_2Al_3 single crystal as used in [1, 2]. At low fields, a very sharp peak in $M(H)$ is found at the lower critical field H_{c1}, which is of the order of $\simeq 100$ Oe only. Furthermore a hysteretic peak in the magnetization curve shows up above H_i as high as 30 kOe (as $T \to 0$ K). This anomaly resembles the shape of magnetization loops found in superconductors with a pronounced peak effect in the critical current density j_c [5]. Most remarkably, the magnetization process is reversible over a wide field range, i.e., 10 kOe $< H < H_i$. Such a reversible magnetization curve is highly unusual and has only been observed in extremely clean type-II superconductors, e.g., in Nb ($\kappa \simeq 0.8$) with a resistance ratio of 1830 [6]. This indicates that the pinning force for the magnetic vortices is very weak. On the other hand, the occurrence of the "peak effect" above H_i, even for the large value of $\kappa \simeq 50$, highlights a very strong pinning force in UPd_2Al_3. In this publication we want to relate this spontaneous increase of the pinning force in the case of UPd_2Al_3 as well as of some other type-II superconductors, all of which show large spin susceptibilities, to a phase transformation from the mixed state into a new inhomogeneous superconducting state. Besides UPd_2Al_3, another heavy-fermion compound, UPt_3 [7], as well as two (strongly) intermediate-valent compounds, $CeRu_2$ [8–12] and V_3Si [13, 14] are known to show a similar magnetization process.

The compounds mentioned above belong to the class of clean type-II superconductors with very large Ginzburg-Landau parameter, κ. They exhibit large spin susceptibilities, and the field H_i at which the "peak effect" occurs is almost equal to the paramagnetically limited field $H_p = \Delta_0/\sqrt{2}\mu_B$ as shown for UPd_2Al_3, $CeRu_2$, UPt_3, and V_3Si in Table 1 [15]. Under these circumstances, one expects the occurrence of a new inhomogeneous superconducting state in which at the cost of superconducting condensation energy the system gains spin-polarization energy. For this state, Fulde and Ferrell [3] were the first to propose an order parameter whose phase is varying in space with a wave number Q. In this state the superconducting energy gap disappears at some part of the Fermi surface. In the Fulde-Ferrell state the electron spins are uniformly polarized in real space. Larkin and Ovchinnikov [4] considered an order parameter of the form $\Delta(z) = \Delta \sin Qz$ which has planar nodes in real space. The spin polarization appears around these nodes. Burkhardt and Rainer [33] treated the Fulde-Ferrell-Larkin-Ovchinnikov (FFLO) state for quasi-two-dimensional

* Dedicated to Professor Peter Fulde on the occassion of his 60th birthday

layered superconductors in the magnetic field parallel to the layers and calculated the spatially varying order parameter and spin polarization of a function of an applied magnetic field. In the above models the orbital or vortex current is not included, and the magnetic field acts only on the spins of the conduction electrons. Gruenberg and Gunther [34] calculated the upper critical field for the Fulde-Ferrell state in type-II superconductors taking into account the orbital current and assuming that the phase transition from the normal state to the Fulde-Ferrell state is of second order. They showed that the critical field exceeds that of the usual mixed state at temperatures below 0.56 T_c in the strong paramagnetic limit.

In this paper, we calculate the superconducting order parameter by including both the effects of strong spin polarization and orbital current. The calculation shows that a new inhomogeneous state appears in a certain range of temperature and magnetic field. In this state the superconducting order parameter is periodically modulated along the direction of the vortices. The structure of the order parameter consists of a periodic array of planar nodes perpendicular to the vortices. We will argue that, on the basis of this superconducting structure, the "peak effect" in the magnetization process and other anomalous properties related to the "peak effect" are naturally explained.

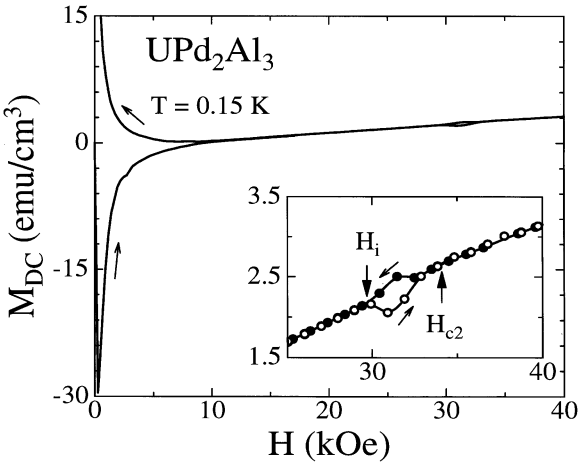

Fig. 1. Low-T magnetization of UPd_2Al_3 single crystal ($T_c = 1.83$ K) measured by a SQUID magnetometer at $T = 0.15$ K ($H \| [0\,0\,1]$). Inset shows magnification of the hysteresis loop below H_{c2}

In order to obtain the new inhomogeneous superconducting state we use a formulation invoking an inhomogeneous spin density. Before setting up this formulation, let us explain that the reversible magnetization process below H_i can be naturally understood within the present model. The superconducting order parameter in the mixed state vanishes inside the vortex cores, causing a loss of the superconducting condensation energy. This loss is counted as the vortex-core energy in conventional superconductors. However, in those superconductors having a large spin susceptibility, we should add to the vortex-core energy an additional contribution from the spin polarization inside the vortex core. The spin susceptibility of the conduction electrons, recovered inside the vortex core, causes a decrease of the magnetic energy. This magnetic energy is expressed by $-(1/2)\chi_{\text{spin}}h^2$ where h is the magnetic field induced at the vortex core by the current surrounding it. If we approximate the vortex core by a cylinder whose radius equals the coherence length $r \simeq \xi_0$, the vortex-core energy per unit length is given by

$$E_{\text{core}} = \pi\xi_0^2\left[\frac{H_c^2}{8\pi} - \frac{1}{2}\chi_{\text{spin}}h^2\right]. \tag{1.1}$$

The vortex core energy is very small in the compounds considered here, since ξ_0 is short. As seen in Table 1, we find that, at high magnetic field near H_{c2}, the loss of the

Table 1. Physical parameters in the normal and superconducting states of heavy-fermion and intermediate-valence superconductors. Values for H_{c1}, H_{c2}, H_p and H_i are taken for $T \to 0$ K

Material	T_c (K)	l (nm)	ξ_0 (nm)	κ	χ_{spin} (10^{-5} $\frac{\text{emu}}{\text{cm}^3}$)	H_{c1} ($\oslash$e)	H_{c2} (10^4 $\oslash$e)	H_P[a] (10^4 $\oslash$e)	H_i (10^4 $\oslash$e)	$\frac{1}{2}\chi_{\text{spin}}H_{c2}^2$ (10^3 $\frac{\text{erg}}{\text{cm}^3}$)	$H_c^2/8\pi$ (10^3 $\frac{\text{erg}}{\text{cm}^3}$)
UPd_2Al_3	2[17]	72[18]	8.5[17]	50[18]	3.2[19]	100[20]	3.6 $\| c$[20] 3.2 $\| a$[20]	3.4	3 $\| c$[20] 2.7 $\| a$[20]	20.6 $\| c$ 16.4 $\| a$	18.3[c, 21]
$CeRu_2$	6.04[20]	130[b]	6.1[8]	16[8]	2.7 ± 0.5[d]	250[10]	7.0[10]	≤ 7.9[20]	4.1[20]	66 ± 12	<84[8, e]
V_3Si	16.9[f]	30[f]	3[22]	20[22]	4.5 ± 1.35[f]	700[13]	$\simeq 20.0$[13]	21.9 ± 2.7	$\simeq 14$[13]	900 ± 300	1080
UPt_3	0.48[23]	200[24]	14.0 $\| c$[24] 12.0 $\| a$	90[25]	9.4 $\| c$[26] 18.8 $\| a$[26]	7.1[25]	1.9 $\| c$[27] 2.3 $\| a$[27]	1.1 $\| c$ 0.78 $\| a$	1.7 $\| c$[7]	17.0 $\| c$ 49.7 $\| a$	5.7[c, 25]
UBe_{13}	0.9[16]	16.5[25]	9.5[28]	60[28]	17.0[29]	46[28]	14.0[16]	1.7	—	1670	25[c, 16]
UNi_2Al_3	1[31]	47[18]	24[18]	14[18]	4.2[31]	90[25]	0.99[32]	1.6	—	2.1	8.1[c, 31]
$CeCu_2Si_2$	0.7[28]	≤ 27[28]	9.0[28]	53[28]	5.6[30]	23[28]	2.5 $\| c$[28] 2.1 $\| a$[28]	1.3	—	17.5 $\| c$ 12.3 $\| a$	24.4[c, 28]

[a] Estimated from χ_{spin} via $H_p = H_c/2\sqrt{\pi\chi_{\text{spin}}}$; for H_c, cf. (c). [b] Y. Ōnuki, unpublished results. [c] Estimated via $H_c^2/8\pi = 0.25(\gamma_0/V_{\text{mole}})T_c^2$. [d] Low-T spin-dependent susceptibility, after correction for diamagnetic core and Landau contributions[8]. χ_{spin} includes both the intrinsic Pauli susceptibility and an extrinsic "impurity" contribution, presumably due to 0.2 at % "non-transformed" Ce^{3+} ions. [e] Upper limit of the condensation-energy density, not taking into account pair breaking by 0.2 at % "non-transformed" Ce^{3+} ions. [f] crystal # 5 of [13]

superconducting condensation energy is almost canceled by the gain of the spin-polarization energy. That is, the vortex-core energy expressed by Eq. (1.1) almost vanishes at high magnetic fields. In this case the vortex-core pinning force due to impurities and imperfections becomes extremely weak. This fact explains the reversible magnetization process occurring in a wide range of the mixed state below H_i. The lower critical field is given by

$$H_{c1} = \frac{4\pi}{\Phi_0}\left[E_{\text{core}} + \frac{\Phi_0}{8\pi}\, h\right], \tag{1.2}$$

where $\Phi_0 = hc/2|e|$. The second term in the brackets of Eq. (1.2) is the vortex-current contribution which is also small due to the large penetration depth in the compounds. From Eq. (1.2) we also expect a very small H_{c1} consistent with the experimental results, see Table 1.

On the other hand, in the inhomogeneous state above H_i, the vortices are cut by the planar nodes of the order parameter and they become flexible in a similar way to those in high-T_c superconductors. The flexible vortices are efficiently pinned by pinning centers due to the collective pinning mechanism [35]. The "peak effect" above H_i can be explained by this pinning.

2. Formulation

If quasiparticles are strongly scattered by the spin-orbit interaction due to impurities, spins are polarized by an external magnetic field without the occurrence of the inhomogeneous state mentioned in the Introduction [36, 37]. Therefore, for the inhomogeneous state to occur, the quasiparticle mean free path l_{so} caused by spin-orbit scattering at impurities should be sufficiently larger than the superconducting coherence length ξ_0 (as $T \to 0$ K). Actually, this condition is fulfilled in samples which we concern, since the samples are clean (large total quasiparticle mean free paths l) and coherence lengths of the samples are short, i.e., $l_{so} > l > \xi_0$. Therefore, we start with the following BCS Hamiltonian of the clean limit which includes the Zeeman term, taking into account the action of the magnetic field on the quasiparticle spins

$$\begin{aligned} H = & \int d^3r \sum_\sigma \psi_\sigma^\dagger(\mathbf{r}) \\ & \times\left[-\frac{\hbar}{2m}\left(\nabla + \frac{2ie}{\hbar c}\mathbf{A}\right)^2 - \mu + \frac{1}{2}\, g\sigma\mu_B B(\mathbf{r})\right]\psi_\sigma(\mathbf{r}) \\ & - \int d^3r d^3r' (\Delta(\mathbf{r},\mathbf{r}')\psi_\uparrow^\dagger(\mathbf{r})\psi_\downarrow^\dagger(\mathbf{r}') + \Delta^*(\mathbf{r},\mathbf{r}')\psi_\downarrow(\mathbf{r}')\psi_\uparrow(\mathbf{r})), \end{aligned} \tag{2.1}$$

where $\psi_\sigma(\mathbf{r})$ is the annihilation operator of a quasiparticle with spin variable σ, g is its g-factor, $\mathbf{A}$ the vector potential, μ the chemical potential, μ_B the Bohr magneton, and $\mathbf{B} = \nabla\times\mathbf{A}$ the magnetic induction. In the present calculation we take $g = 2$, the free-electron value for simplicity. If spin-singlet pairing state is assumed, then the superconducting order parameter is expressed by

$$\begin{aligned} &\Delta(\mathbf{r},\mathbf{r}') = \Delta(\mathbf{r})\delta(\mathbf{r}-\mathbf{r}'), \\ &\Delta(\mathbf{r}) = V\langle\psi_\downarrow(\mathbf{r})\psi_\uparrow(\mathbf{r})\rangle, \end{aligned} \tag{2.2}$$

where V is the pairing strength.

As shown by Eilenberger [38], the equations for the Gor'kov Green's functions F, F^+, and G are transformed into much simpler equations by using a quasiclassical approximation. By integrating F, F^+, and G over the conduction-electron energy $\xi_{\mathbf{k}}$, Eilenberger introduced the functions f, f^+, and g

$$f(\mathbf{r},\hat{\mathbf{k}}_F,\omega_s) = \int\frac{d\xi_{\mathbf{k}}}{2\pi}\, F(\xi_{\mathbf{k}},\hat{\mathbf{k}}_F,\omega_s;\Delta(\mathbf{r}),\mathbf{A}(\mathbf{r})), \tag{2.3a}$$

$$f^+(\mathbf{r},\hat{\mathbf{k}}_F,\omega_s) = \int\frac{d\xi_{\mathbf{k}}}{2\pi}\, F^+(\xi_{\mathbf{k}},\hat{\mathbf{k}}_F,\omega_s;\Delta(\mathbf{r}),\mathbf{A}(\mathbf{r})), \tag{2.3b}$$

$$g(\mathbf{r},\hat{\mathbf{k}}_F,\omega_s) = \int\frac{d\xi_{\mathbf{k}}}{2\pi}\, G(\xi_{\mathbf{k}},\hat{\mathbf{k}}_F,\omega_s;\Delta(\mathbf{r}),\mathbf{A}(\mathbf{r})), \tag{2.3c}$$

where $\omega_s = \omega_l + \mathrm{i}\mu_B B$ with $\omega_l = (2l+1)\pi T$ and $\hat{\mathbf{k}}_F$ is the unit vector in the direction of the Fermi momentum $\mathbf{k}_F$. For a clean superconductor, these functions satisfy the following Eilenberger equations

$$\left[\omega_l + i\mu_B B + \frac{v_F}{2}\,\hat{\mathbf{k}}_F\cdot\Pi\right] f(\mathbf{r},\hat{\mathbf{k}}_F,\omega_s) = \Delta(\mathbf{r}) g(\mathbf{r},\hat{\mathbf{k}}_F,\omega_s), \tag{2.4}$$

$$\left[\omega_l + i\mu_B B - \frac{v_F}{2}\,\hat{\mathbf{k}}_F\cdot\Pi^\dagger\right] f^+(\mathbf{r},\hat{\mathbf{k}}_F,\omega_s) = \Delta^*(\mathbf{r}) g(\mathbf{r},\hat{\mathbf{k}}_F,\omega_s), \tag{2.5}$$

$$g(\mathbf{r},\hat{\mathbf{k}}_F,\omega_s) = \sqrt{1 - f(\mathbf{r},\hat{\mathbf{k}}_F,\omega_s) f^+(\mathbf{r},\hat{\mathbf{k}}_F,\omega_s)}, \quad (\mathrm{Re}\, g > 0) \tag{2.6}$$

where

$$\Pi = \nabla + \frac{2ei}{\hbar c}\,\mathbf{A}(\mathbf{r}), \quad \Pi^\dagger = \nabla - \frac{2ei}{\hbar c}\,\mathbf{A}(\mathbf{r}). \tag{2.7}$$

We have assumed a spherical Fermi surface, v_F being the Fermi velocity. Equations (2.4) and (2.5) are completed by two self-consistency equations for the order parameter $\Delta(\mathbf{r})$ and the magnetic field $\mathbf{B}(\mathbf{r})$. The self-consistency equations for $\Delta(\mathbf{r})$ of Eq. (2.2) is rewritten as

$$\begin{aligned} \Delta(\mathbf{r})\ln\frac{T}{T_c} + 2\pi T\sum_{l=0}^{\infty}\Bigg[&\frac{\Delta(\mathbf{r})}{\omega_l} \\ &- \frac{1}{2}\int\frac{d^2\hat{k}_F}{4\pi}\left(f(\mathbf{r},\hat{\mathbf{k}}_F,\omega_s) + f(\mathbf{r},\hat{\mathbf{k}}_F,\omega_s^*)\right)\Bigg] = 0, \end{aligned} \tag{2.8}$$

where T_c is the transition temperature at zero field. The magnetic field $\mathbf{B}(\mathbf{r})$ is calculated from the current expression

$$\begin{aligned} \nabla\times(\mathbf{B}(\mathbf{r}) - \mathbf{H}) &= \frac{4\pi}{c}\,\mathbf{j}(\mathbf{r}) \\ &= \frac{8\pi e}{\hbar c}\, 2\pi T N(0)\times\sum_{l=0}^{\infty}\int\frac{d^2\hat{k}_F}{4\pi}\, v_F\hat{\mathbf{k}}_F\,\mathrm{Im}\, g(\mathbf{r},\hat{\mathbf{k}}_F,\omega_s), \end{aligned} \tag{2.9}$$

where H is an external magnetic field in the direction of the z axis. In deriving Eqs. (2.8) and (2.9), we have used the

symmetry relations which follow from Eqs. (2.4)–(2.6):

$$f^*(\mathbf{r}, \hat{\mathbf{k}}_F, \omega_s) = f^+(\mathbf{r}, \hat{\mathbf{k}}_F, -\omega_s^*),$$
$$g^*(\mathbf{r}, \hat{\mathbf{k}}_F, \omega_s) = -g(\mathbf{r}, \hat{\mathbf{k}}_F, -\omega_s^*), \tag{2.10a}$$
$$f^*(\mathbf{r}, \hat{\mathbf{k}}_F, \omega_s) = f^+(\mathbf{r}, -\hat{\mathbf{k}}_F, \omega_s^*),$$
$$g^*(\mathbf{r}, \hat{\mathbf{k}}_F, \omega_s) = g(\mathbf{r}, -\hat{\mathbf{k}}_F, \omega_s^*), \tag{2.10b}$$
$$f(\mathbf{r}, \hat{\mathbf{k}}_F, \omega_s) = f(\mathbf{r}, -\hat{\mathbf{k}}_F, -\omega_s),$$
$$g(\mathbf{r}, \hat{\mathbf{k}}_F, \omega_s) = -g(\mathbf{r}, -\hat{\mathbf{k}}_F, -\omega_s), \tag{2.10c}$$

The Gibbs free-energy functional G which is defined by the difference between the Gibbs free energies of the superconducting and the normal state is given by

$$G = \int d^3r \left\{ \frac{1}{8\pi}(B(\mathbf{r}) - H)^2 + |\Delta(\mathbf{r})|^2 N(0) \ln \frac{T}{T_c} + \pi T N(0) \sum_{l=-\infty}^{\infty} \left[\frac{|\Delta(\mathbf{r})|^2}{|\omega_l|} - \int \frac{d^2\hat{k}_F}{4\pi} I(\mathbf{r}, \hat{\mathbf{k}}_F, \omega_s) \right] \right\}, \tag{2.11}$$

with

$$I(\mathbf{r}, \hat{\mathbf{k}}_F, \omega_s) = \Delta f^+ + \Delta^* f + \left(g - \frac{\omega_l}{|\omega_l|} \right) \times \left\{ \frac{1}{f} \left[\omega_s + \frac{v_F}{2} \hat{\mathbf{k}}_F \cdot \mathbf{\Pi} \right] f + \frac{1}{f^+} \left[\omega_s - \frac{v_F}{2} \hat{\mathbf{k}}_F \cdot \mathbf{\Pi}^\dagger \right] f^+ \right\}, \tag{2.12}$$

where the arguments $\mathbf{r}$, $\mathbf{v}_F$, and ω_s of f, f^+ are omitted for brevity. If we require G being stationary under variation of f^+, f, Δ^*, and $\mathbf{A}$, we obtain Eqs. (2.4), (2.5), (2.8), and (2.9), respectively. Inserting Eqs. (2.4) and (2.5) into Eq. (2.11), we have

$$G = \int d^3r \left\{ \frac{1}{8\pi}(B(\mathbf{r}) - H)^2 + |\Delta(\mathbf{r})|^2 N(0) \ln \frac{T}{T_c} + 2\pi T N(0) \sum_{l=0}^{\infty} \times \left[\frac{|\Delta(\mathbf{r})|^2}{\omega_l} - \mathrm{Re} \int \frac{d^2\hat{k}_F}{4\pi} \frac{\Delta(\mathbf{r}) f^+(\mathbf{r}, \hat{\mathbf{k}}_F, \omega_s) + \Delta^*(\mathbf{r}) f(\mathbf{r}, \hat{\mathbf{k}}_F, \omega_s)}{1 + g(\mathbf{r}, \hat{\mathbf{k}}_F, \omega_s)} \right] \right\}. \tag{2.13}$$

Near H_{c2}, we linearize the Eilenberger equations (2.4) and (2.5) with respect to $\Delta(\mathbf{r})$. A stable solution of the equations is

$$\Delta(\mathbf{r}) = \Psi(\mathbf{r}_\perp) \sin Qz, \quad \mathbf{r}_\perp = (x, y), \tag{2.14a}$$

where $\Psi(\mathbf{r}_\perp)$ is the order parameter of the Abrikosov vortex lattice (cf. Eq. (2.26)) and Q is a wave number. This solution has the nodal planes of the order parameter perpendicular to the vortices. Another possible solution is one in which the nodal planes are parallel to the vortices, and the vortex cores reside in the planes. A calculation shows that H_{c2} for this solution is smaller than for the solution of Eq. (2.14a). This fact indicated that the solution of Eq. (2.14a) is more stable than that of the nodal planes being parallel to the vortices. Below H_{c2} the order parameter is written by

$$\Delta(\mathbf{r}) = \Psi(\mathbf{r}_\perp) \eta(\mathbf{r}_\perp, z), \tag{2.14a}$$

as a generalization of Eq. (2.14a). The function $\eta(\mathbf{r}_\perp, z)$ is determined by solving the Eilenberger equations. The function $\eta(\mathbf{r}_\perp, z)$ being just a function of z. Expanding η and g in a Fourier transform

$$\eta(z) = \sum_n \eta_n e^{inQz}, \tag{2.15}$$

$$g(\mathbf{r}, \hat{\mathbf{k}}_F, \omega_s) = \sum_n g_n(\mathbf{r}_\perp, \hat{\mathbf{k}}_F, \omega_s) e^{inQz}, \tag{2.16}$$

and inserting these quantities into the Eilenberger equation (2.4), we obtain

$$f(\mathbf{r}, \hat{\mathbf{k}}_F, \omega_s) = \sum_{n,m} \frac{\eta_n e^{i(n+m)Qz}}{\omega_s + (v_F/2)\hat{\mathbf{k}}_\perp \cdot \mathbf{\Pi}_\perp + (i/2)(n+m)Qv_F \cos\theta} \times \Psi(\mathbf{r}_\perp) g_m(\mathbf{r}_\perp, \hat{\mathbf{k}}_F, \omega_s), \tag{2.17}$$

where $\hat{\mathbf{k}}_\perp$ and $\mathbf{\Pi}_\perp$ are the components of $\hat{\mathbf{k}}_F$ and $\mathbf{\Pi}$ perpendicular to the z axis, respectively, and θ is the polar angle of $\hat{\mathbf{k}}_F$. In Eq. (2.17) we neglect the z component $\mathbf{A}_z$ since the current along the z axis j_z may be very small for the FFLO state with a sinusoidal oscillation along the z axis. Note that $\mathbf{\Pi}_\perp$ in the denominator operates on both $\Psi(\mathbf{r}_\perp)$ and $g_m(\mathbf{r}_\perp, \hat{\mathbf{k}}_F, \omega_s)$. Near H_{c2}, where the order parameter is small, the leading contribution comes from a term of $\mathbf{\Pi}_\perp$ operating on $\Psi(\mathbf{r}_\perp)$ since $g \sim 1 - \mathrm{O}(\Delta^2)$. Therefore, we may neglect the operation of $\mathbf{\Pi}_\perp$ on g_m: $\mathbf{\Pi}_\perp$ operates only on $\Psi(\mathbf{r}_\perp)$. In order to proceed further from Eq. (2.17), we introduce the operators

$$a = \frac{\xi_H}{\sqrt{2}\, i}(\mathbf{\Pi}_x - i\mathbf{\Pi}_y), \quad a^\dagger = \frac{\xi_H}{\sqrt{2}\, i}(\mathbf{\Pi}_x + i\mathbf{\Pi}_y), \tag{2.18}$$

where

$$\xi_H = \left(\frac{\hbar c}{2eH} \right)^{1/2}. \tag{2.19}$$

The operators a and $a^\dagger$ satisfy the commutation relation

$$[a, a^\dagger] = B(\mathbf{r})/H, \tag{2.20}$$

which enables us to express $\mathbf{\Pi}_\perp^2$ in terms of a and $a^\dagger$ as

$$-\mathbf{\Pi}_\perp^2 = \frac{2}{\xi_H^2} \left(a^\dagger a + \frac{1}{2} \frac{B(\mathbf{r})}{H} \right). \tag{2.21}$$

The magnetic field $B(\mathbf{r})$ may be written as

$$B(\mathbf{r}) = H + h_s(\mathbf{r}) + 4\pi m(\mathbf{r}), \tag{2.22}$$

where h_s is the field due to the supercurrent and $m(\mathbf{r})$ is the magnetization due to the spin polarization of the quasiparticles. For fields near H_{c2} where the peak effect occurs, $h_s(\mathbf{r})$ and $4\pi m(\mathbf{r})$ are of order of 10 Oe, while H is of order of 10^4 Oe, so that $B(\mathbf{r})/H$ in Eqs. (2.20) and (2.21) is almost unity near H_{c2}. In the following we put $B(\mathbf{r}) = H$ and use the commutation relation $[a, a^\dagger] = 1$.

In terms of a and $a^\dagger$, Eq. (2.17) is written for positive ω_l's as

$$f(\mathbf{r}, \hat{\mathbf{k}}_F, \omega_s) = \frac{2}{v_F} \int_0^\infty d\rho \exp\left[-\left(\frac{2\omega_s}{v_F} + \frac{i(ae^{i\varphi} + a^\dagger e^{-i\varphi})}{\sqrt{2}\xi_H} \sin\theta \right) \rho \right] \Psi(\mathbf{r}_\perp) \times \eta(z - \rho\cos\theta) g(\mathbf{r}_\perp, z - \rho\cos\theta, \hat{\mathbf{k}}_F, \omega_s), \tag{2.23}$$

where φ is the azimuthal angle of $\hat{\mathbf{k}}_F$, $\hat{\mathbf{k}}_F$ being expressed by the polar and azimuthal angles as

$$\hat{\mathbf{k}}_F = (\sin\theta\cos\varphi, \sin\theta\sin\varphi, \cos\theta). \tag{2.24}$$

We see from Eqs. (2.20) and (2.21) that a and $a^\dagger$ are the creation and annihilation operators of a harmonic oscillator. We take $\Psi_n(\mathbf{r}_\perp)$ to be a solution to the equation for the oscillator

$$-\mathbf{\Pi}_\perp^2 \Psi_n(\mathbf{r}_\perp) = \frac{2}{\xi_H^2}(a^\dagger a + \tfrac{1}{2})\Psi_n(\mathbf{r}_\perp) = \frac{2}{\xi_H^2}(n+\tfrac{1}{2})\Psi_n(\mathbf{r}_\perp), \tag{2.25}$$

n being an integer ($n \geq 0$). The solution for the lowest Landau level ($n = 0$) is given in the form which has an Abrikosov vortex-lattice structure

$$\Psi_0(\mathbf{r}_\perp) = \sum_n C_n e^{-ina_V y/\xi_H^2} \exp\left[-\frac{(x-na_V)^2}{2\xi_H^2}\right], \tag{2.26}$$

where a_V is the vortex spacing in the direction of the x axis and C_n a periodic function on n, i.e., $C_{n+\nu} = C_n$ for a certain integer ν. For the triangular vortex lattice, $\nu = 2$ and $C_1 = iC_0$. In the following we restrict ourselves to the lowest Landau level, i.e., we use $\Psi_0(\mathbf{r}_\perp)$ for $\Psi(\mathbf{r}_\perp)$ in Eq. (2.23).

If we substitute Eq. (2.26) into Eq. (2.23) and use the identities

$$\exp[ca - c^* a^\dagger] = e^{-c^* a^\dagger} e^{ca} \exp(-|c|^2/2), \quad e^{ca}\Psi_0(\mathbf{r}_\perp) = 0, \tag{2.27}$$

where $c = -i\rho\sin\theta/\sqrt{2}\xi_H$, Eq. (2.23) is rewritten as

$$f(\mathbf{r}, \hat{\mathbf{k}}_F, \omega_s) = \frac{2}{v_F}\int_0^\infty d\rho \exp\left[-\frac{2\omega_s}{v_F} - \left(\frac{\rho\sin\theta}{2\xi_H}\right)^2\right] \times g(\mathbf{r}_\perp, z-\rho\cos\theta, \hat{\mathbf{k}}_F, \omega_s) \times \eta(z-\rho\cos\theta)\exp\left[-i\frac{\rho\sin\theta}{\sqrt{2}\xi_H}a^\dagger e^{-i\varphi}\right]\Psi_0(\mathbf{r}_\perp). \tag{2.28}$$

If we use Eq. (2.28) in the gap equation (2.8), the terms of the higher Landau levels generated by $\exp[-i(\rho\sin/\sqrt{2}\xi_H)a^\dagger e^{-i\varphi}]\Psi_0(\mathbf{r}_\perp)$ vanish when integrating with respect to φ in the gap equation, so that we retain the lowest Landau level only in Eq. (2.28), yielding

$$f(\mathbf{r}, \hat{\mathbf{k}}_F, \omega_s) = \Psi_0(\mathbf{r}_\perp)\frac{2}{v_F}\int_0^\infty d\rho \exp\left[-\frac{2\omega_s}{v_F}\rho - \left(\frac{\rho\sin\theta}{2\xi_H}\right)^2\right] \times \eta(z-\rho\cos\theta) g(\mathbf{r}_\perp, z-\rho\cos\theta, \hat{\mathbf{k}}_F, \omega_s). \tag{2.29}$$

In a similar way, we obtain the expression for f^+

$$f^+(\mathbf{r}, \hat{\mathbf{k}}_F, \omega_s) = \Psi_0^*(\mathbf{r}_\perp)\frac{2}{v_F}\int_0^\infty d\rho \exp\left[-\frac{2\omega_s}{v_F}\rho - \left(\frac{\rho\sin\theta}{2\xi_H}\right)^2\right] \times \eta^*(z+\rho\cos\theta) g(\mathbf{r}_\perp, z+\rho\cos\theta, \hat{\mathbf{k}}_F, \omega_s). \tag{2.30}$$

We note that the functions f and f^+ in Eqs. (2.29) and (2.30) are proportional to $\Psi_0(\mathbf{r}_\perp)$ and $\Psi_0^*(\mathbf{r}_\perp)$, respectively.

It is still difficult to solve the Eqs. (2.29) and (2.30) numerically, so that we make a further approximation to these equations. We notice from Eqs. (2.6), (2.29), and (2.30) that $g(\mathbf{r}_\perp, z, \hat{\mathbf{k}}_F, \omega_s)$ depends on $\mathbf{r}_\perp$ through its functional dependence of $|\Psi_0(\mathbf{r}_\perp)|^2$. We replace $|\Psi_0(\mathbf{r}_\perp)|^2$ in g with its spatial average $\langle|\Psi_0(\mathbf{r}_\perp)|^2\rangle$:

$$\langle|\Psi_0(\mathbf{r}_\perp)|^2\rangle = \int \frac{d^3r}{\Omega}|\Psi_0(\mathbf{r}_\perp)|^2, \tag{2.31}$$

where Ω is the volume of the system. Then, it is convenient to introduce the $\mathbf{r}_\perp$-independent new functions $\tilde{f}(z, \hat{\mathbf{k}}_F, \omega_s)$ and $\tilde{f}^+(z, \hat{\mathbf{k}}_F, \omega_s)$ defined by

$$\tilde{f}(z, \hat{\mathbf{k}}_F, \omega_s) = f(\mathbf{r}, \hat{\mathbf{k}}_F, \omega_s)/\tilde{\Psi}_0(\mathbf{r}_\perp). \tag{2.32}$$

$$\tilde{f}^+(z, \hat{\mathbf{k}}_F, \omega_s) = f^+(\mathbf{r}, \hat{\mathbf{k}}_F, \omega_s)/\tilde{\Psi}_0^*(\mathbf{r}_\perp), \tag{2.33}$$

with the normalized order parameter of the Abrikosov vortex lattice

$$\tilde{\Psi}_0(\mathbf{r}_\perp) = \frac{\Psi_0(\mathbf{r}_\perp)}{\sqrt{\langle|\Psi_0(\mathbf{r}_\perp)|^2\rangle}}. \tag{2.34}$$

In terms of $\tilde{f}$, $\tilde{f}^+$, and $\tilde{g}$, we rewrite the Eilenberger equations (2.29) and (2.30) as

$$\tilde{f}(z, \hat{\mathbf{k}}_F, \omega_s) = \frac{2}{v_F}\int_0^\infty d\rho \exp\left[-\frac{2\omega_s}{v_F}\rho - \left(\frac{\rho\sin\theta}{2\xi_H}\right)^2\right] \times \tilde{\eta}(z-\rho\cos\theta)\tilde{g}(z-\cos\theta, \hat{\mathbf{k}}_F, \omega_s), \tag{2.35}$$

$$\tilde{f}^+(z, \hat{\mathbf{k}}_F, \omega_s) = \frac{2}{v_F}\int_0^\infty d\rho \exp\left[-\frac{2\omega_s}{v_F}\rho - \left(\frac{\rho\sin\theta}{2\xi_H}\right)^2\right] \times \tilde{\eta}^*(z+\rho\cos\theta)\tilde{g}(z+\cos\theta, \hat{\mathbf{k}}_F, \omega_s), \tag{2.36}$$

where

$$\tilde{g}(z, \hat{\mathbf{k}}_F, \omega_s) = \sqrt{1-\tilde{f}(z, \hat{\mathbf{k}}_F, \omega_s)\tilde{f}^+(z, \hat{\mathbf{k}}_F, \omega_s)}, \tag{2.37}$$

$$\tilde{\eta}(z) = \sqrt{\langle|\Psi_0(\mathbf{r}_\perp)|^2\rangle}\eta(z). \tag{2.38}$$

By noting that $\Delta(\mathbf{r})$ is expressed as

$$\Delta(\mathbf{r}) = \tilde{\Psi}_0(\mathbf{r}_\perp)\tilde{\eta}(z), \tag{2.39}$$

the gap equation (2.8) is reduced to the gap equation for $\tilde{\eta}$

$$\tilde{\eta}(z)\ln\frac{T}{T_c} + 2\pi T \times \sum_{l=0}^\infty \left[\frac{\tilde{\eta}(z)}{\omega_l} - \frac{1}{2}\int\frac{d^2\hat{\mathbf{k}}_F}{4\pi}(\tilde{f}(z, \hat{\mathbf{k}}_F, \omega_s) + \tilde{f}(z, \hat{\mathbf{k}}_F, \omega_s^*))\right] = 0. \tag{2.40}$$

The Gibbs free energy G in Eq. (2.13) is rewritten as

$$G = N(0)\int dz \left\{|\tilde{\eta}(z)|^2 \ln\frac{T}{T_c} + 2\pi T\sum_{l=0}^\infty \times \left[\frac{|\tilde{\eta}(z)|^2}{\omega_l} - \mathrm{Re}\int\frac{d^2\hat{k}_F}{4\pi}\frac{\tilde{\eta}(z)\tilde{f}^+(z, \hat{\mathbf{k}}_F, \omega_s) + \tilde{\eta}^*(z)\tilde{f}(z, \hat{\mathbf{k}}_F, \omega_s)}{1+\tilde{g}(z, \hat{\mathbf{k}}_F, \omega_s)}\right]\right\}. \tag{2.41}$$

Equations (2.35), (2.36), and (2.40) are self-consistently solved by numerical computation. The solutions of $\tilde{f}$, $\tilde{f}^{+}$, $\tilde{g}$ and $\tilde{\eta}(z)$ are used to calculate the Gibbs free energy and several physical quantities, which are presented in Sect. 3 and Sect. 5, respectively.

3. Nature of the generalized FFLO state

We look for a solution of the Eilenberger equations (2.35) and (2.36) and the gap equation (2.40) by assuming that $\tilde{\eta}(z)$ varies periodically along the z direction

$$\tilde{\eta}(z) = \tilde{\eta}(z + \Lambda), \tag{3.1}$$

Λ being the wave length of the oscillation. The functions $\tilde{f}$, $\tilde{f}^{+}$, and $\tilde{g}$ have the same periodicity as $\eta(z)$ in the z direction. We numerically solve the Eilenberger equations and the gap equation self-consistently in the region $0 < z < \Lambda$ by using the relaxation method. The solutions $\tilde{f}$, $\tilde{f}^{+}$, $\tilde{g}$, and $\tilde{\eta}(z)$ are used to calculate the Gibbs free energy, Eq. (2.41). The wave length Λ is determined by minimizing the Gibbs free energy with respect to Λ.

We introduce a parameter α which characterizes the strength of the spin paramagnetic effect relative to the orbital effect [39]:

$$\alpha = \frac{H_{c2}^{(orb)}}{\sqrt{2}e^{2+\gamma}H_p}, \tag{3.2}$$

where $\gamma = 0.57721$ is the Euler constant, $H_{c2}^{(orb)} = (e^{2+\gamma}/\pi^2)(\Phi_0/2\pi\xi_0^2)$ is the orbital critical field in the clean limit, and $H_p = \Delta_0/\sqrt{2}\mu_B$. Here ξ_0 is the superconducting coherence length defined by $\xi_0 = \hbar v_F/\pi\Delta_0$, Δ_0 being the superconducting order parameter at $H = 0$ and $T = 0$. The temperature is fixed to $T/T_c = 0.15$ throughout the remainder of this paper.

In Fig. 2, we show the numerical results of $\tilde{\eta}(z)$ as a function of z for $\alpha = 2$. The order parameter $\Delta(\mathbf{r})$ is proportional to $\tilde{\eta}(z)$ (see Eq. (2.39)), so that $\Delta(\mathbf{r})$ has the same z dependence as $\tilde{\eta}(z)$. For an external magnetic field near H_{c2}, the order parameter oscillates nearly sinusoidally along the z axis. As the magnetic field decreases, the shape of the order parameter changes to a rectangular one. The spatial and field dependence of $\tilde{\eta}(z)$ in Fig. 2 is quite similar to the results obtained by Burkhardt and Rainer [33] and Machida and Nakanishi [40], although the vortices do not exist in their model. In the present model, the order parameter has spatial variation of the Abrikosov vortex-lattice structure in the xy plane as well as the amplitude oscillation along the z axis. This is a *field-induced layered structure* with the vortices perpendicular to the nodes. A schematic diagram of this state is shown in Fig. 3, in which the solid lines show the center of the vortices and the dashed lines show the planar nodes of the superconducting order parameter perpendicular to the vortices. We call the superconducting state having the structure shown in Fig. 3 the *generalized FFLO state* (referred to as the GFFLO state). The GFFLO state resembles the vortex state of layered oxide superconductors in magnetic fields perpendicular to the CuO_2 planes.

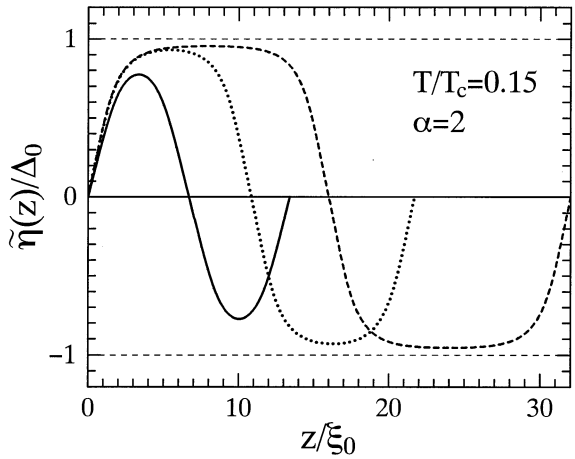

Fig. 2. Spatial variation of $\tilde{\eta}$ along the z axis as a function of z/ξ_0. The solid, dotted, and dashed curves indicate $\tilde{\eta}$ for $\mu_B H/\Delta_0 = 0.725$, 0.690, and 0.680, respectively. Each curve is plotted over one period of Λ

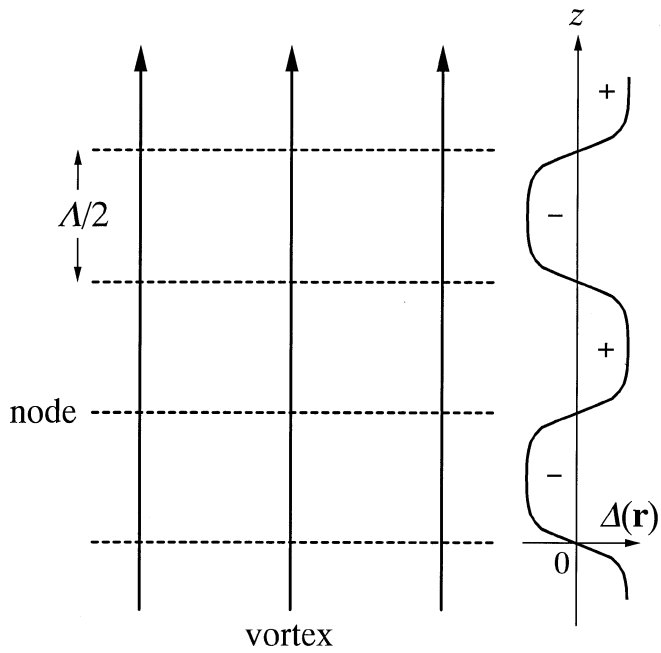

Fig. 3. Schematic diagram of the GFFLO state. The vertical solid lines represent the center of the vortices and the horizontal dotted lines represent the nodal planes of the superconducting order parameter. The figure on the right side represents the spatial variation of the gap amplitude along the z axis

The difference between the Gibbs free energies of the GFFLO state and the normal state is shown for $\alpha = 1$ and $\alpha = 2$ in Figs. 4 and 5, respectively. The dashed line shows the free energy of the vortex state, and the solid line shows the free energy of the GFFLO state. When the external magnetic field increases, the superconductor undergoes a first-order phase transition at H_i from the vortex state to the GFFLO state [41]. The phase transition from the GFFLO state to the normal state at H_{c2} is also of first order. In Figs. 6 and 7 the wavelength, Λ, of the order parameter in units of the coherence length, ξ_0, is shown as

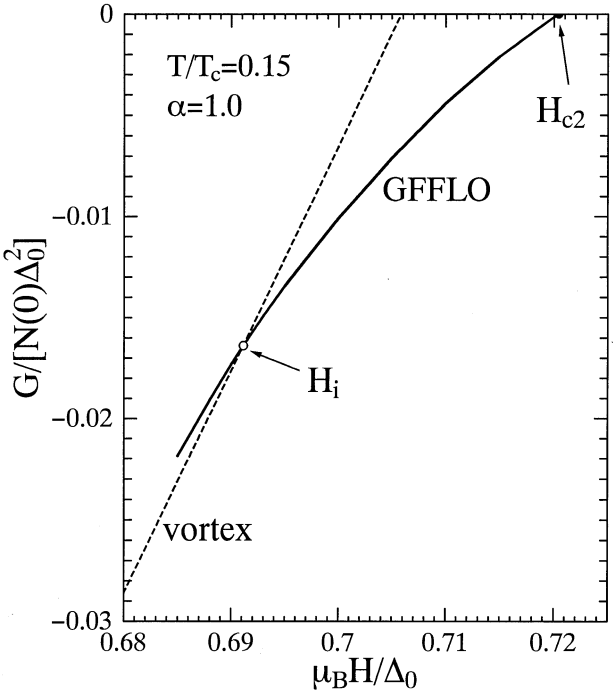

Fig. 4. Normalized Gibbs free energy of the GFFLO state relative to that of the normal state for $\alpha = 1$. The dashed line shows the free energy of the Abrikosov vortex state, and the solid line shows the free energy of the GFFLO state. The open and solid circles indicate first-order phase transition points betweeen the vortex state and the GFFLO state and between the GFFLO state and the normal state, respectively

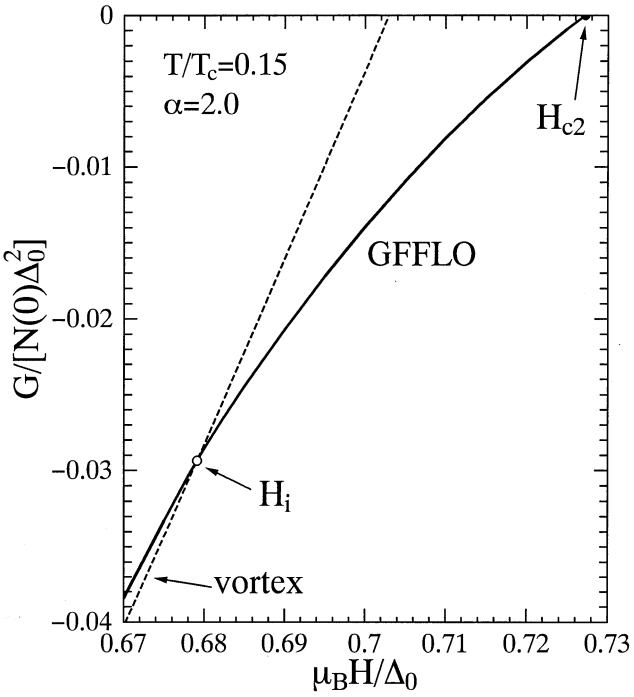

Fig. 5. Normalized Gibbs free energy of the GFFLO state relative to that of the normal state for $\alpha = 2$. Lines and circles have the same meaning as in Fig. 4

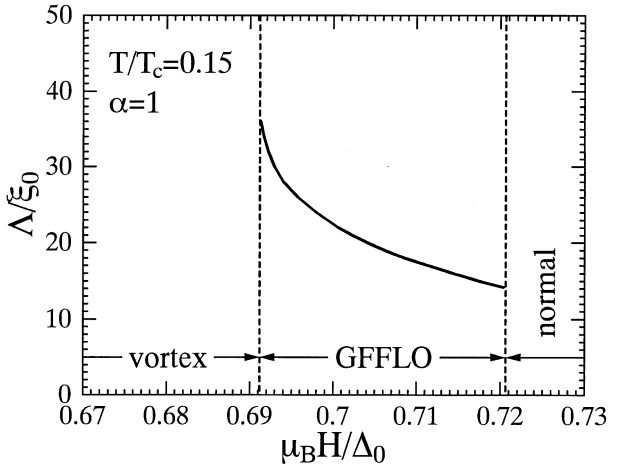

Fig. 6. Wave length, Λ, of the order parameter along the z axis as a function of $\mu_B H/\Delta_0$ for $\alpha = 1$

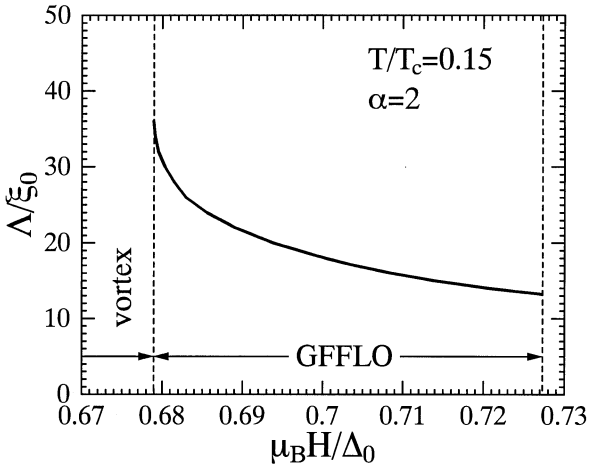

Fig. 7. Wave length, Λ, of the order parameter along the z axis as a function of $\mu_B H/\Delta_0$ for $\alpha = 2$

function of the external magnetic field. The coherence length, ξ_0, is 8.5 nm and 6.1 nm for UPd_2Al_3 and $CeRu_2$, respectively. The wave length increases as the magnetic field decreases and attains a maximum at H_i.

In our calculation the GFFLO state appears when α is larger than the critical value of $\alpha_{cr} \approx 0.07$. If we literally use the values of ξ_0 and H_p in Table 1 in α of Eq. (3.2b), α is estimated to be 0.093 for UPd_2Al_3 and 0.087 for $CeRu_2$, both of which exceed the critical value α_{cr} [42]. However, these values are too small to explain the phase diagram of UPd_2Al_3 and $CeRu_2$. The expression (3.2) for α may be inadequate to these materials, since it is derived by use of a simple quasi-free electron model. For quantitative discussions, we need to develop our theory by taking into account the electronic structure characteristic for heavy-fermion and intermediate-valence compounds.

4. Comparison with experiments

As discussed in the Introduction, the pinning force acting on straight (rigid) vortices in these clean superconductors

with enhanced spin-susceptibility is very weak. In the GFFLO state, however, we expect a significant change in the pinning capability of the superconductor. Here the occurrence of planar nodes of the order parameter leads to a segmentation of the vortices into pieces with a length of several times the coherence length. As a result, these vortex segments become flexible in a qualitatively similar way as the quasi-two-dimensional vortex disks ("pancakes") in high-T_c superconductors. If the vortices are subject to weak disorder as, e.g., in the presence of point defects, we expect the individual vortex segments to accommodate more easily to the random pinning potential, thereby becoming efficiently pinned by the collective action of weak pinning centers.

Below we communicate experimental results on single crystalline $CeRu_2$, which besides those on UPd_2Al_3 (cf. Figure 1 and [20]) provide strong indication for the realization of the GFFLO state, i.e., the existence of a first-order phase transition in the mixed state at high magnetic fields, accompanied by an abrupt increase in the pinning capability.

Figure 8 shows an isothermal dc-magnetization curve of a $CeRu_2$ single crystal as a function of magnetic field. For details of the measuring procedure we refer to [20]. As for UPd_2Al_3 (cf. Fig. 1) the magnetization process is found to be reversible over a wide field range, i.e., $19\ \text{kOe} < H < H_i(T) = 33\ \text{kOe}$ at $T = 3$ K, indicative of a macroscopically pinning-free vortex state at intermediate field strength. For fields $H > H_i(T)$, however, we observe an abrupt increase of the diamagnetic response. This anomaly, along with the paramagnetic peak showing up with decreasing field, indicates the creation of shielding currents as a consequence of trapped flux inside the superconductor. Further evidence for a strongly pinned vortex state above $H_i(T)$ stems from the observations of a sharp negative peak in the in-phase component of the ac-susceptibility (see [8] and [43–45] for results on $CeRu_2$ and UPd_2Al_3, respectively) as well as from the occurrence of pronounced anomalies in the magnetostriction: Figure 9 displays field-induced length changes $\Delta l(H)$ of our $CeRu_2$ single crystal measured under isothermal conditions at various temperatures. The observation of an

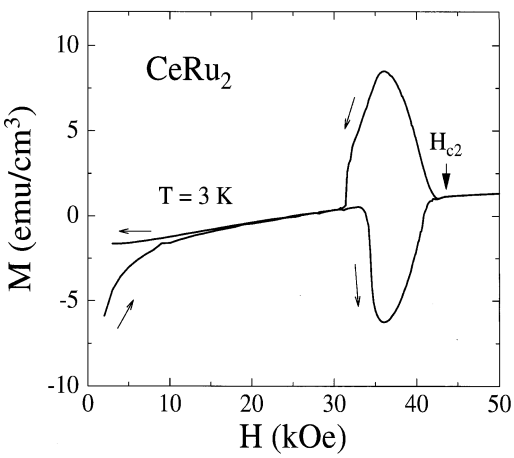

Fig. 8. Isothermal dc-magnetization curve of a $CeRu_2$ single crystal, measured by a SQUID magnetometer at $T = 3$ K ($H \parallel [1\,1\,0]$)

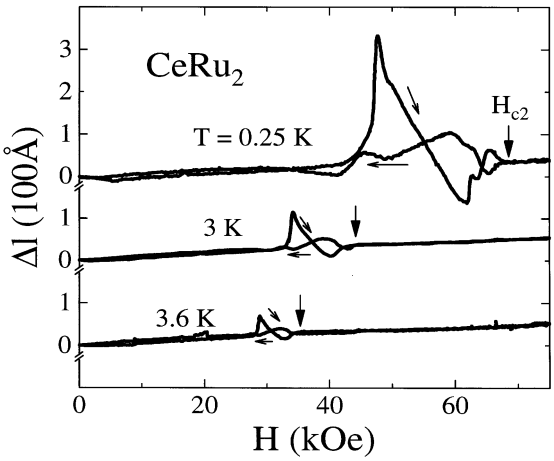

Fig. 9. Magnetostriction data, Δl vs H, of a $CeRu_2$ single crystal (length $l = 3.25$ mm) at three different temperatures ($H \parallel [0\,0\,1]$). Vertical arrows indicate $H_{c2}(T)$ determined from magnetization measurements

abrupt change from a smooth and reversible magnetization process for $H < H_i(T)$ to a behavior with pronounced field-induced length changes of hysteretic nature above $H_i(T)$ strongly hints at the onset of flux pinning, i.e., at the coupling of the vortex lattice to the crystal lattice above $H_i(T)$. The strong decrease of the amplitude of the $\Delta l(H)$ anomaly with increasing temperature (cf. Fig. 9) has also been observed for UPd_2Al_3 [1, 2]. As can be seen in Fig. 9 the anomalous structure in $\Delta l(H)$ becomes very small at $T = 3.6$ K, and for temperatures above $T = 5.5$ K, corresponding to $T/T_c = 0.9$, no anomaly can be resolved anymore. This is in line with the T-dependence of the amplitude of the magnetization loop [20].

The abrupt increase of flux pinning above H_i, and moreover, the significant hysteresis in H_i upon increasing and decreasing field (Figs. 8 and 9) are strong indications for a first-order transition at H_i.

5. Predictions for other physical properties

In the following we wish to calculate various physical quantities in order to elucidate the properties of the generalized GFFLO state in more detail.

A. Spin polarization

The spin density of quasiparticles defined by $\langle\sigma\rangle = \langle\psi_\uparrow^\dagger\psi_\uparrow\rangle - \langle\psi_\downarrow^\dagger\psi_\downarrow\rangle$ is calculated from the expression

$$\langle\sigma\rangle = 2\mu_B H N(0) - 4\pi N(0) T \sum_{l=0}^{\infty} \int \frac{d^2\hat{k}_F}{4\pi} \operatorname{Im}[\tilde{g}(z, \hat{\mathbf{k}}_F, \omega_s)]. \tag{5.1}$$

This expression is quite well approximated by the formula

$$\langle\sigma\rangle \approx \sigma_N \left(1 - \left[\frac{\Delta(\mathbf{r})}{\Delta_0}\right]^2\right), \tag{5.2}$$

if the calculated values of $\Delta(\mathbf{r})$ are used in Eq. (5.2). In Eq. (5.2), σ_N denotes the spin polarization in the normal state, $2\mu_B BN(0)$. The spin polarization appearing around the nodes of the order parameter is shown in Fig. 10. In Fig. 10 the spin polarization is normalized by σ_N. The wave length of the spin-density wave is $\Lambda/2$. The maximum value of the spin-density is slightly larger than that in the normal state. The spin polarization direction is antiparallel to the magnetic field. The spatial and field dependence of $\langle\sigma\rangle$ are similar to those obtained by Burkhardt and Rainer [33] and Machida and Nakanishi [40] in the FFLO state. In the present case the spins are also polarized in the vortex cores. The magnetic moments corresponding to σ_N are approximately 0.013 μ_B and 0.011 μ_B per molecule of UPd_2Al_3 and $CeRu_2$, respectively. The spin polarization is expected to be observable by neutron-diffraction experiments in a paramagnetic metal like $CeRu_2$.

B. Local density of states

In the GFFLO state, we expect a bound state around the nodes of the order parameter, since the order parameter changes its sign at the nodes. The quasiparticle density of states with spin σ, $N_\sigma(\omega)$, calculated from the expression

$$N_\sigma(\omega) = N(0)\int \frac{d^2\hat{k}_F}{4\pi}\,\mathrm{Re}[\,\tilde{g}(z,\hat{\mathbf{k}}_F,\omega-\sigma\mu_B H)\,], \tag{5.3}$$

where σ takes $\uparrow$ or $+$ for up spins and $\downarrow$ or $-$ for down spins. In Eq. (5.3), the function $\tilde{g}$ depends on a real frequency ω, while in previous sections we obtained $\tilde{g}$ as a function of the imaginary frequency $i\omega_\ell$. In order to obtain $\tilde{g}$ as a function of a real frequency ω, we analytically continue the function $\tilde{g}$ on the imaginary frequency axis to the real frequency axis using the Páde approximation [46]. The local density of states associated with the bound state is shown in Fig. 11. In Fig. 11 we see the sharp peaks split by $2\mu_B H$, which may be observed in the $I-V$ characteristics as taken by a scanning tunneling microscope.

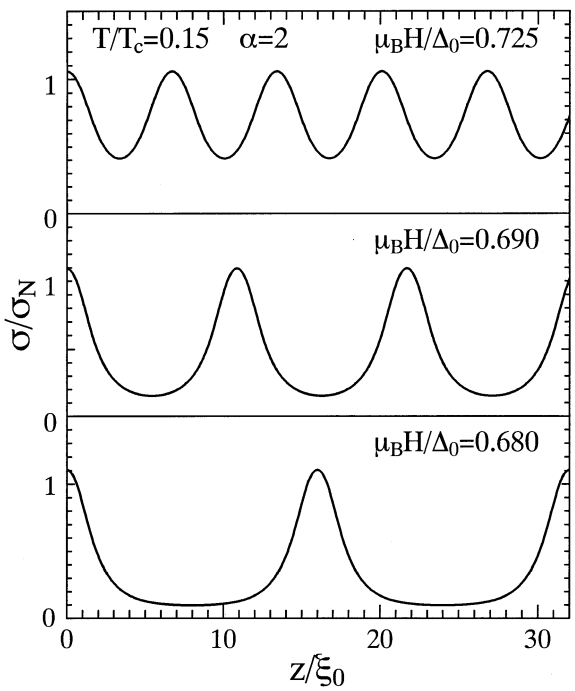

Fig. 10. Spin-density wave induced in the GFFLO state for three different magnetic fields. The spin density σ is normalized to that in the normal state, σ_N. The peaks of σ correspond to the nodes of the supercondcuting order parameter

C. Supercurrent passing through nodes

For the GFFLO state with the sinusoidal oscillation $\Delta(\mathbf{r}) = \Delta_Q\cos(Qz)$, a question arises as to whether the supercurrent can flow in the direction of the z axis. According to the Ginzburg-Landau theory, the supercurrent cannot pass through the nodal planes where the order parameter is vanishing, since in the GL theory the supercurrent is proportional to the square of the order parameter. It should be noted that the validity of the GL theory is restricted to temperatures near T_c, while the GFFLO state appears near H_{c2} well below T_c where the nonlocal effect plays a crucial role for the current response. Since the presence of the vortices is not relevant to

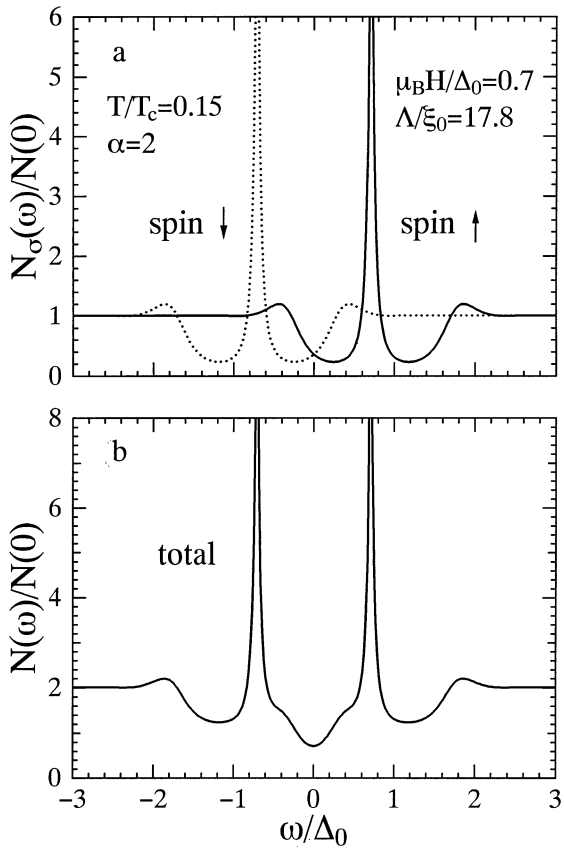

Fig. 11a, b. Local density of states at the position of a planar node of the superconducting order parameter as a function of energy. The upper panel shows the local density of states for the up and down spins by the solid and dashed curves, respectively, and the lower panel shows the sum of them, i.e., the total local density of states

answer the above question, we neglect the vortices for simplicity.

Near H_{c2}, the staggered order parameter is well approximated by

$$\Delta(z) = \Delta_Q \cos(Qz) e^{i\phi(z)}, \tag{5.4}$$

where $\phi(z)$ is the phase of the order parameter. In the following, we look for a GFFLO state carrying a uniform current flowing along the z axis when the phase varies linearly in z:

$$\phi(z) = a \frac{z}{\xi_0}, \tag{5.5}$$

where a is a dimensionless constant. In the close vicinity of H_{c2} in the GFFLO state, $\Delta(\mathbf{r})$ is small, so that we may expand g up to second order in Δ_Q:

$$g(z, \hat{\mathbf{k}}_F, \omega_s) \sim 1 - (1/2) f(z, \hat{\mathbf{k}}_F, \omega_s) f^+(z, \hat{\mathbf{k}}_F, \omega_s), \tag{5.6}$$

where f and f^+ are given by

$$f(z, \hat{\mathbf{k}}_F, \omega_s) = \frac{2}{v_F} \int_0^\infty d\rho \exp\left[-\frac{2\omega_s}{v_F} \rho \right] \Delta(z - \rho\cos\theta), \tag{5.7}$$

$$f^+(z, \hat{\mathbf{k}}_F, \omega_s) = \frac{2}{v_F} \int_0^\infty d\rho \exp\left[-\frac{2\omega_s}{v_F} \rho \right] \Delta^*(z + \rho\cos\theta), \tag{5.8}$$

Equations (5.7) and (5.8) indicate the nonlocal relationships between the function f and the order parameter $\Delta(z)$ and between f^+ and $\Delta(z)$. Using Eqs. (5.4)–(5.8) in the current expression (2.9), we have the supercurrent in the direction of z as

$$j_z = \frac{3}{16} n_e e v_F \left(\frac{\Delta_0}{\varepsilon_F}\right)\left(\frac{\Delta_Q}{\Delta_0}\right)^2 (I_1 + I_2 \cos(2Qz)), \tag{5.9}$$

with

$$I_1 = -2\pi T \Delta_0 \mathrm{Im} \sum_{\ell=0}^{\infty} \int_{-1}^{1} \frac{dx}{2} \times \left\{ \frac{x}{[\omega_s + (i/2) v_F Q_+ x]^2} + \frac{x}{[\omega_s - (i/2) v_F Q_- x]^2} \right\}, \tag{5.10}$$

$$I_2 = -2\pi T \Delta_0 \mathrm{Im} \sum_{\ell=0}^{\infty} \int_{-1}^{1} \frac{dx}{2} \times \frac{2x}{[\omega_s + (i/2) v_F Q_+ x][\omega_s - (i/2) v_F Q_- x]}, \tag{5.11}$$

where n_e is the electron density, ε_F is the Fermi energy, $Q_\pm = Q \pm a/\xi_0$, and $x = \cos\theta$. At $T = 0$, I_1 and I_2 are calculated as

$$I_1 = -\frac{1}{\pi Q_+ \xi_0}\left(2 - \alpha_+ \ln\left|\frac{1+\alpha_+}{1-\alpha_+}\right|\right) - \frac{1}{\pi Q_- \xi_0}\left(2 - \alpha_+ \ln\left|\frac{1-\alpha_-}{1+\alpha_-}\right|\right), \tag{5.12}$$

$$I_2 = -\frac{1}{\pi Q \xi_0}\left(\ln\left|\frac{1-\alpha_-^2}{1-\alpha_+^2}\right| - \alpha_- \ln\left|\frac{1-\alpha_-}{1+\alpha_-}\right| - \alpha_+ \ln\left|\frac{1+\alpha_+}{1-\alpha_+}\right| + 2\ln\left|\frac{Q_-}{Q_+}\right|\right), \tag{5.13}$$

where

$$\alpha_\pm = \frac{2\mu_B H}{v_F Q_\pm}. \tag{5.14}$$

Note that Eqs. (5.12) and (5.13) are valid for $\alpha_- \ll 1$, i.e., $a \ll \xi_0 Q(1 - 2\mu_B H/Q v_F)$.

A uniform current j_z is achieved by putting the second term in the brackets in Eq. (5.11) zero:

$$I_2(Q, a) = 0. \tag{5.15}$$

This equation determines Q as a function of a. For small a and $T = 0$, the condition (5.15) is rewritten from Eq. (5.13) as

$$\alpha \ln\left|\frac{1+\alpha}{1-\alpha}\right| = 2, \quad \alpha = \frac{2\mu_B H}{v_F Q}. \tag{5.16}$$

Equations (5.16) has a solution of $\alpha = 0.8334$, yielding the relation $Q = 2.40(\mu_B H/v_F)$. This expression is the same as that obtained from the condition, $\partial H_{c2}(Q)/\partial Q = 0$, the nucleation field ($H_{c2}$) having the maximum value.

For small values of a, using $\alpha = 0.8334$, the supercurrent j_z at $T = 0$ is expressed up to first order in a as

$$j_z = 1.34 n_e e v_F a \left(\frac{\Delta_0}{\varepsilon_F}\right)\left(\frac{\Delta_Q}{\Delta_0}\right)^2 \left(\frac{\Delta_0}{\mu_B H}\right)^2. \tag{5.17}$$

Equation (5.17) shows that the supercurrent can flow passing through the nodes of the superconducting order parameter by inducing the phase gradient a/ξ_0 in Eq. (5.5)

6. Discussion

We have chosen UPd_2Al_3 and $CeRu_2$ to illustrate the unique properties predicted by our theory. As already mentioned in the Introduction, UPt_3 [7] and V_3Si [13, 14] are further candidates to show the GFFLO state. Recently, the proposal was made to explain the highly unusual $H_{c2}(T)$ curve of the heavy-fermion superconductor UBe_{13} by a strong-coupling theory [16]. This treatment includes an FFLO state to account for the occurrence of extremely large $H_{c2}(T)$ values at very low temperatures ($H_{c2}(T \to 0) \simeq 140$ kOe [16]). As Table I shows, UBe_{13} like UPt_3 indeed fulfills the requirement of a large Zeeman energy. On the other hand, for the heavy-fermion superconductor UNi_2Al_3, the Zeeman energy is too small compared to the superconducting condensation energy. Consequently, one finds no anomalies related to the GFFLO state for this compound [47, 48]. The case of $CeCu_2Si_2$, on the other hand, shows that near equality of the condensation and zeeman energies is necessary, but not sufficient for the anomalous "peak effect" to be observed: Here, strong pinning in the whole Shubnikov phase [48] and no GFFLO-related anomalies [48, 49] were found.

The $H - T$ phase diagrams of both UPd_2Al_3 [2, 20] and $CeRu_2$ [8–12, 20] suggest a surprisingly large existence range of the GFFLO state, i.e., $T < T_i \approx 0.9\, T_c$. This range is much more extended than the one obtained by those models assuming quasi-free electrons [3, 4, 33, 34, 50]. In addition, the magnetic field range, in which the

GFFLO state exists, exceeds the theoretical prediction substantially (cf. [35, 50–53]). Future investigations which have to take into account realistic g factors and band structures for the renormalized carriers are expected to resolve these remaining problems. In particular, antiferromagnetic exchange interactions between the quasiparticles can enlarge the field region of the GFFLO state as was discussed by Burkhardt and Rainer [33]. Antiferromagnetic quasiparticle–quasiparticle interactions preferentially occur either in the presence of nesting properties or for a multiply-connected Fermi surface in general. In fact, for both UPd_2Al_3 and $CeRu_2$ de-Haas-van-Alphen measurements [54, 55] and band-structure calculations [55–57] reveal nearly disjunct portions of the Fermi surface. Concerning the onset of the GFFLO state at $T = T_i$, this should be reflected by an increase in the slope of $H_{c2}(T)$. Interestingly enough, this feature is clearly resolved in the $H - T$ phase diagram of $CeRu_2$ [8–12, 20], while it is not visible for UPd_2Al_3 [2, 20].

The present theory shows that the phase transition from the GFFLO into the normal state at $H_{c2}(T)$ at intermediate temperatures (except for high temperatures and extremely low temperatures) is of weakly first order [58], in contrast to conventional type-II superconductors. However, in our experiments this transition appears to be of second order.

Finally, let us make a general comment on the observability of the GFFLO state in heavy-fermion superconductors, which are frequently assumed to exhibit unconventional order parameters. In Sect. 2, we assumed a spin-singlet s-wave ($l = 0$) pairing superconductor. However, the present result can as well be applied to a qualitative discussion for a spin-singlet d-wave ($\ell = 2$) pairing superconductor [59].

The authors would like to express their sincere thanks to A.A. Abrikosov, G.W. Crabtree, T. Fujita, P. Fulde, K. Gloos, K. Kadowaki, T. Koyama, J. Kübler, M.B. Maple, H. Matsumoto, and D. Rainer for stimulating conversations, M. Deppe and J.L. Tholence for their experimental support as well as T. Komatsubara and N. Sato for providing the single-crystalline UPd_2Al_3 sample. Two of the authors (M.T. and S.T.) are also indebted to Y. Tanaka and S. Kasiwaya for their discussions of the bound state discussed in Sect. 5.B. This work was supported by a Grant-in-Aid for Scientific Research on Priority Area, "Science of High-T_c Superconductivity" given by the Ministry of Education, Science and Culture, Japan, and by the Super-Computing Center of the Institute for Materials Research, Tohoku University. The part of the work done at Darmstadt was supported by the Deutsche Forschungsgemeinschaft under the auspices of the Sonderforschungsbereich 252 Darmstadt/Frankfurt/Mainz.

References

1. Modler, R., Gloos, K., Geibel, C., Komatsubara, T., Sato, N., Schank, C., Steglich, F.: Int. J. Mod. Phys. B**7**, 42 (1993); Modler, R.: diploma thesis, Darmstadt (1992), unpublished
2. Gloos, K., Modler, R., Schimanski, H., Bredl, C.D., Geibel, C., Steglich, F., Buzdin, A.I., Sato, N., Komatsubara, T.: Phys. Rev. Lett. **70**, 501 (1993)
3. Fulde, P., Ferrell, R.A.: Phys. Rev. **135**, 550 (1964)
4. Larkin, A.I., Ovchinnikov, Yu. N.: Zh. Eksp. Teor. Fiz. **47**, 1136 (1964) [Sov. Phys. JETP **20**, 762 (1965)]
5. Campbell, A.M., Evetts J.E.: Adv. Phys. **21**, 327 (1972)
6. Finnemore, D.K., Stromberg, T.F., Swenson, C.A.: Phys. Rev. **149**, 231 (1966); Weber, H.W., Seidl, E., Laa, C., Schachinger, M., Prohammer, M., Junod, A., Eckert, D.: Phys. Rev. B **44**, 7858 (1991)
7. Tenya, K., Ikeda, M., Tayama, T., Mitamura, H., Amitsuka, H., Sakakibara, T., Maezawa, K., Kimura, N., Settai, R., Ōnuki, Y.: J. Phys. Soc. Jpn. **64**, 1063 (1995)
8. Huxley, A.D., Paulsen, C., Laborde, O., Tholence, J.L., Sanchez, D., Junod, A., Calemczuk, R.: J. Phys.: Condens. Matter **5**, 7709 (1993)
9. Yagasaki, K., Hedo, M., Nakama, T.: J. Phys. Soc. Jpn. **62**, 3825 (1993)
10. Sugawara, H., Yamazaki, T., Kimura, N., Settai, R., Ōnuki, Y.: Physica C **206**–**207**, 196 (1995)
11. Goshima, H., Suzuki, T., Fujita, T., Hedo, M., Nakama, T., Yagasaki, K.: Physica C **206**–**207**, 193 (1995)
12. Kadowaki, K., Hirata, K., Takeya, H.: (preprint 1995)
13. Isino, M., Kobayashi, T., Toyota, N., Fukase, T., Muto, Y.: Phys. Rev. B **38**, 4457 (1988)
14. Uehara, M.: (private communication)
15. The large susceptibilities of the u-based compounds mag indicate substantial, if not dominating, orbital contributions. The astonishing discrepancy between the Zeeman and condensation energies in the case of UBe_{13} is related to the highly unusual $H_{c2}(T)$ behavior of this compound [16]
16. Thomas, F., Wand, B., Lühmann, T., Gegenwart, P., Stewart, G.R., Steglich, F., Brison, J.P., Buzdin, A.I., Glemot, L., Flouquet, J.: J. Low Temp. Phys. (in press)
17. Geibel, C., Schank, C., Thies, S., Kitazawa, H., Bredl, C.D., Böhm, C.D., Rau, M., Grauel, A., Caspary, R., Helfrich, R., Ahlheim, U., Weber, G., Steglich, F.: Z. Phys. B **84**, (1991)
18. Steglich, F., Ahlheim, U., Böhm, C.D., Bredl, C.D., Caspary, R., Geibel, C., Grauel, A., Helfrich, R., Köhler, R., Lang, M., Mehner, A., Modler, R., Schank, C., Wassilew, C., Weber, G., Assmus, W., Sato, N., Komatsubara, T.: Physica C **185**–**189**, 379 (1991)
19. χ_{spin} corresponds to $\cong 2 \cdot 10^{-3}$ emu/mole characterizing the "superconducting 5f subsystem": Feyerherm R., Amato, A., Gygax, F.N., Schenk, A., Geibel, C., Steglich, F., Sato, N., Komatsubara, T.: Phys. Rev. Lett. **73**, 1849 (1994)
20. Steglich, F., Modler, R., Gegenwart, P., Deppe, M., Weiden, M., Lang, M., Geibel, C., Lühmann, T., Paulsen, P., Tholence, J.L., Ōnuki, Y., Tachiki, M., Takahashi, S.: Physica C (in press)
21. $\gamma_0 = 115\ \mathrm{mJ/K^2\ mol}$, characterizing the "superconducting 5f subsystem" has been used: Caspary, R., Hellmann, P., Keller, M., Sparn, G., Wassilew, C., Köhler, R., Weber, G., Geibel, C., Schank, C., Steglich, F., Phillips, N.E.: Phys. Rev. Lett. **71**, 2146 (1993)
22. Orlando, T.P., McNiff, E.J. Jr., Foner, S., Beasley, M.R.: Phys. Rev. B **19**, 4545 (1979)
23. de Visser, A., Menovsky, A.A., Franse, J.J.M.: Physica B **147**, 81 (1987)
24. Yin, G., Maki, K.: Phys. Rev. Lett. **47**, 892 (1993)
25. Koziol, Z.: Ph.D. Thesis, Amsterdam (1994) (unpublished)
26. Frings, P.H., Franse, J.J.M., de Boer, F.R., Menovsky, A.A.: J. Mag. Mag. Mat. **31**–**34**, 1595 (1983)
27. van Dijk, N.H., de Visser, A., Franse, J.J.M., Taillefer, L.: J. Low Temp. Phys. **93**, 101 (1993)
28. Rauchschwalbe, U.: Physica B **147**, 1 (1987)
29. Ott, H.R., Rudigier, H., Fisk, Z., Smith, J.L.: Phys. Rev. Lett. **50**, 1595 (1983)
30. Lieke, W., Rauchschwalbe, U., Bredl, C.D., Steglich, F., Aarts, J., de Boer, F.R.: J. Appl. Phys. **63**, 2111 (1982)
31. Geibel, C., Thies, S., Kaczorowski, Grauel, A., Seidel, A., Ahlheim, U., Helfrich, R., Petersen, K., Bredl, C.D., Steglich, F.: Z. Phys. B **83**, 305 (1991); χ_{spin} has been estimated by an extrapolation of the normal-state susceptibility below T_N to $T \to 0$
32. Dalichaouch, Y., de Andrade, M.C., Maple, M.B.: Phys. Rev. B **46**, 8671 (1992)
33. Burkhardt, H., Rainer, D.: Ann. Phys. **3**, 181 (1994)
34. Gruenberg, L.W., Gunther, L.: Phys. Rev. Lett. **16**, 996 (1966)

35. Larkin, A.I., Ovchinnikov Yu.N.: J. Low Temp. Phys. **34**, 409 (1979)
36. Ferrell, R.A.: Phys. Rev. Lett. **3**, 262 (1959)
37. Anderson, P.W.: Phys. Rev. Lett. **3**, 325 (1959)
38. Eilenberger, G.: Z. Phys. **214**, 195 (1966)
39. Note that α differs from α_{GG} in [34] $\alpha/\alpha_{GG} = (2\varepsilon^{2+\gamma})^{-1}$
40. Machida, K. and Nakanishi, H.: Phys. Rev. B **30**, 122 (1995)
41. Burkhardt and Rainer [33] have shown in their two-dimensional model the transition from the FFLO state to the uniform superconducting state is of second order. The presence of the vortices suppresses the mixing of the higher harmonics of the order parameter in the GFFLO state. The suppression makes the phase transition from the GFFLO state to the pure vortex state to be of first order
42. In Figs. 4–7, $\alpha = 1$, and $\alpha = 2$, respectively, were chosen in order to enlarge the field range of the GFFLO state
43. Lühmann, T., Gegenwart, P., Reinders, P.H., Geibel, C., Steglich, F., Paulsen, C., Tholence, J.L.: Physica C **235**–**240**, 95 (1994)
44. Steglich, F., Geibel, C., Gloos, K., Hellmann, P., Köhler, R., Lang, M., Modler, R., Schank, C.: Physica C **235**–**240**, 95 (1994)
45. Ishiguro, A., Sawada, A., Kimura, J., Suzuki, M., Sato, N., Komatsubara, T.: J. Phys. Soc. Jpn. **64**, 378 (1995)
46. Vidberg, H.J., Serene, J.W.: J. Low Temp. Phys. **29**, 179 (1977)
47. Modler, R., Lang, M., Geibel, C., Schank, C., Steglich, F.: Physica **B199**–**200**, 145 (1994)
48. Gegenwart, P.: Diploma Thesis, TH Darmstadt (1994) (unpublished)
49. Modler, R.: Dissertation, TH Darmstadt (1995) (unpublished)
50. Norman, M.R.: Phys. Rev. Lett. **71**, 3391 (1993)
51. Aoi, K., Dieterich, W., Fulde, P.: Z. Phys. **267**, 223 (1974)
52. Shimahara, H.: Phys. Rev. B **50**, 12760 (1995)
53. Dupuis, N.: Phys. Rev. B **51**, 9074 (1995)
54. Inada, Y., Ishiguro, A., Kimura, J., Sato, N., Sawada, A., Komatsubara, T.: Physica C **206-207**, 33 (1995)
55. Hedo, M., Inada, Y., Ishida, T., Yamamoto, E., Haga, Y., Ōnuki, Y., Higuchi, M., Hasegawa, A. J. Phys. Soc. Jpn. (submitted for publication)
56. Sandratskii, L.M., Kübler, J., Zahn, P., Mertig, I.: Phys. Rev. B **50**, 15834 (1995)
57. Yanase, A.: J. Phys. F.: Met. Phys. **16**, 1501 (1986)
58. We can show, in the strong paramagnetic limit of $\alpha \to \infty$, that the phase transition at H_{c2} is of first order in the temperature range of $0.1317 < T/T_c < 0.5615$. Our calculation shows that in a two-dimensional system the phase transition at H_{c2} is of second order in the whole temperature range below T_c, which is consistent with the result of [33]
59. Matsuo, S., Shimahara, H., Nagai, K.: J. Phys. Soc. Jpn. **64**, 371 (1995)